

Catching the bound states in the continuum of a phantom atom in graphene

L. H. Guessi¹, R. S. Machado², Y. Marques², L. S. Ricco², K. Kristinsson³,

M. Yoshida¹, I. A. Shelykh^{3,4,5}, M. de Souza^{1,*} and A. C. Seridonio^{1,2}

¹*IGCE, Unesp - Univ Estadual Paulista, Departamento de Física, 13506-900, Rio Claro, SP, Brazil*

²*Departamento de Física e Química, Unesp - Univ Estadual Paulista, 15385-000, Ilha Solteira, SP, Brazil*

³*Division of Physics and Applied Physics, Nanyang Technological University 637371, Singapore*

⁴*Science Institute, University of Iceland, Dunhagi-3, IS-107, Reykjavik, Iceland*

⁵*ITMO University, St. Petersburg 197101, Russia*

We explore theoretically the formation of bound states in the continuum (BICs) in graphene hosting two collinear adatoms situated at different sides of the sheet and at the center of the hexagonal cell, where a phantom atom of a fictitious lattice emulates the six carbons of the cell. We verify that in this configuration the local density of states (LDOS) near the Dirac points exhibits two characteristic features: i) the cubic dependence on energy instead of the linear one for graphene as found in *New J. Phys.* **16**, 013045 (2014) and ii) formation of BICs as aftermath of a Fano destructive interference assisted by the Coulomb correlations in the adatoms. For the geometry where adatoms are collinear to carbon atoms, we report absence of BICs.

PACS numbers: 72.80.Vp, 07.79.Cz, 72.10.Fk

I. INTRODUCTION

Graphene is a two-dimensional material consisting of an atomic monolayer where carbon atoms build a honeycomb lattice, which is characterized by a band structure exhibiting a massless relativistic dispersion relation in the vicinity of the Dirac cones situated at the corners of the Brillouin zone [1–3]. Recent experimental and theoretical works demonstrated the possibility of the effective controllable adsorption of impurities, the so-called adatoms, by an individual graphene sheet [4–6]. These astonishing hallmarks have driven researchers towards a topic of the electron tunneling through adatoms in a relativistic environment [7–9]. The variety of the adatom geometries considered so far and novel effects predicted are quite broad. For instance, in a system composed by a couple of magnetic adatoms, the exchange coupling results in a highly anisotropic RKKY interaction [10, 11].

In this context, the Scanning Tunneling Microscope (STM) technique has been recognized as the most efficient experimental tool [12]. Its use allows to probe the local density of state (LDOS) of the system. Interestingly enough, the latter is governed by the Fano interference effect [13] between the direct tunneling from the STM tip to the host and that via the adatom. In addition, the Fano effect forms the basis of the appearance of the so-called bound states in the continuum (BICs).

BICs were first theoretically predicted by von Neumann and Wigner in 1929 [14] as quantum states with localized square-integrable wave functions appearing above the threshold of a given stationary potential. The solutions of the corresponding Schrödinger equation are characterized by destructive interference between partial

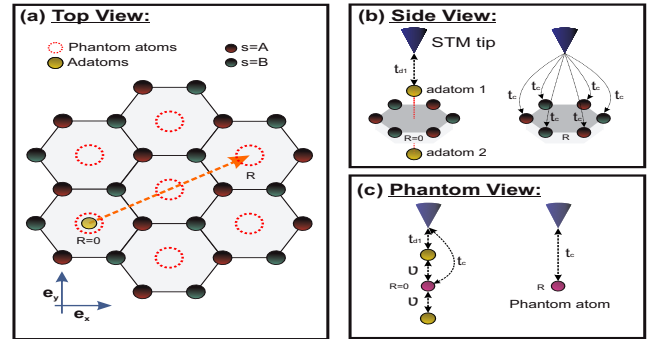


Figure 1. (Color online) The geometry of the system we consider. (a) The dotted-red circles represent a fictitious lattice composed by phantom atoms in graphene. (b) At the position $\mathbf{R} = \mathbf{0}$ the STM tip couples to the adatom 1 and the six atoms of carbon (only shown for an arbitrary \mathbf{R}). (c) Phantom atoms (shaded-red spheres) emulating the cells of (b).

waves which cancel the amplitude of the wave function at large distances from the potential core. Notably, the subject received a revival after the publication of the work of Stillinger and Herrick in 1975 [15]. Since then, appearance of BICs was predicted in optical and photonic systems [16–19], setups with peculiar chirality [20], Floquet-Hubbard states induced by a strong oscillating electric field [21] and driven by A.C. fields [22], among others.

In the domain of the carbon-based structures, graphene ribbons were proposed as appropriate candidates for the detection of BICs [23, 24]. However, from the perspective of quantum transport, such states are difficult to see. Indeed, as the electrons within BICs are not allowed to leak into the continuum, they become invisible in transport experiments. Hence, in order to proof the existence of BICs, proposals of novel experimental setups

* Current address: Institute of Semiconductor and Solid State Physics, Johannes Kepler University Linz, Austria.

suitable for their detection are of fundamental interest.

In this article we discuss theoretically the necessary conditions for the appearance of BICs in graphene-adatom systems. We show that such states appear if two collinear adatoms with Coulomb correlations are placed above and below the center of the hexagonal cell as shown at Fig.1. The situation can be considered by means of the introduction of a fictitious, or phantom atom located at the center of the hexagonal cell and coupled to the STM tip in the transport experiment. In this configuration, the formation of the BIC is assisted by a Fano interference mechanism. Similar process takes place in the optical and photonic systems described in Refs. [17] and [19]. The phantom atom belongs to a fictitious lattice composed by atoms of the same species with DOS presenting a cubic energy dependency as it was originally predicted by B. Uchoa *et al.* [8, 9]. To make the BIC visible, one needs to introduce the mechanism of its coupling with the continuum, which can be done by the use of a detuning between the energy levels of the adatoms.

II. THE MODEL

To give a theoretical description of the setup presented at Fig.1, we develop the model based on the two-impurity Anderson Hamiltonian treated in frameworks of Hubbard I approximation [25]. The system is described by the model Hamiltonian

$$\mathcal{H}_T = \mathcal{H}_{2D} + \mathcal{H}_{\text{tip}} + \mathcal{H}_{\text{tun}}. \quad (1)$$

The first term of \mathcal{H}_T represents the Anderson like-model:

$$\mathcal{H}_{2D} = \mathcal{H}_g + \mathcal{H}_d + \mathcal{H}_\nu, \quad (2)$$

where the first part corresponds to the free graphene sheet

$$\mathcal{H}_g = -t \sum_{\langle \bar{m}, m \rangle \sigma} [\hat{\Psi}_{A\sigma}^\dagger(\mathbf{R}_m) \hat{\Psi}_{B\sigma}(\mathbf{R}_m) + \text{H.c.}] \quad (3)$$

in which $\langle \bar{m}, m \rangle$ runs over the nearest neighbors of carbon atoms with hopping term $t \approx 2.8 \text{ eV}$, $\hat{\Psi}_{s\sigma}^\dagger(\mathbf{R}_m)$ ($\hat{\Psi}_{s\sigma}(\mathbf{R}_m)$) is the creation (annihilation) fermionic operator of an electron for a given spin σ in a sublattice $s = A, B$.

$$\mathcal{H}_d = \sum_{j\sigma} \mathcal{E}_{jd\sigma} n_{d_j\sigma} + \mathcal{U} \sum_j n_{d_j\uparrow} n_{d_j\downarrow} \quad (4)$$

describes the adatoms ($j = 1, 2$), where $n_{d_j\sigma} = d_{j\sigma}^\dagger d_{j\sigma}$, $d_{j\sigma}^\dagger$ ($d_{j\sigma}$) creates (annihilates) an electron with spin σ in the state $\mathcal{E}_{jd\sigma} = \mathcal{E}_d + (-1)^{1-j} \Delta\mathcal{E}$ with the index $j = 1, 2$ designating the upper and lower adatoms respectively, $\Delta\mathcal{E}$ represents the possible detuning between the levels of the different adatoms and \mathcal{U} accounts for the on-site

Coulomb interaction.

$$\mathcal{H}_\nu = \mathcal{V} \sum_{j=1}^2 \sum_{i=1}^3 \sum_{\sigma} \{ [\hat{\Psi}_{A\sigma}(\delta_i) + \hat{\Psi}_{B\sigma}(-\delta_i)] d_{j\sigma}^\dagger + \text{H.c.} \} \quad (5)$$

hybridizes the six atoms of the hexagonal cell with the couple of adatoms as sketched in Fig. 1. $\delta_1 = a\mathbf{e}_x$ and $\delta_{2,3} = \frac{a}{2}(-\mathbf{e}_x \pm \sqrt{3}\mathbf{e}_y)$ represent the nearest neighbor vectors of carbon atoms, $a \sim 1.4 \text{ \AA}$ is the distance between graphene atoms and \mathcal{V} is the hybridization strength, which is supposed to be the same for the six carbons of the hexagonal cell. This assumption holds for adatoms with orbital symmetry s , f_{z^3} and d_{z^2} (Co atoms for instance) [9].

The second part of \mathcal{H}_T is described by the Hamiltonian \mathcal{H}_{tip} , which corresponds to free electrons in the STM tip. The tunneling Hamiltonian, describing the tip-host coupling can be expressed as

$$\begin{aligned} \mathcal{H}_{\text{tun}} &= \sum_{\sigma} [t_c \Psi_{\sigma}(\mathbf{R}) + t_{d1} d_{1\sigma}] \Psi_{\text{tip}\sigma}^\dagger + \text{H.c.} = \\ &= t_c \sum_{\sigma} \tilde{\Psi}_{\sigma}(\mathbf{R}) \Psi_{\text{tip}\sigma}^\dagger + \text{H.c.}, \end{aligned} \quad (6)$$

where $\Psi_{\text{tip}\sigma}$ is the operator for the edge site of the tip and

$$\Psi_{\sigma}(\mathbf{R}) = \sum_{i=1}^3 [\hat{\Psi}_{A\sigma}(\mathbf{R} + \delta_i) + \hat{\Psi}_{B\sigma}(\mathbf{R} - \delta_i)] \quad (7)$$

describes the six carbon atoms of the hexagonal cell with its center collinear to the STM tip position \mathbf{R} as outlined at Fig.1. The field operator

$$\tilde{\Psi}_{\sigma}(\mathbf{R}) = \Psi_{\sigma}(\mathbf{R}) + (t_{d1}/t_c) d_{1\sigma} \quad (8)$$

accounts for the quantum interference between the direct electron tunneling through the carbons of such a cell and tunneling through the adatom 1 placed above the central site of the cell. Note that for the ratio $t_{d1}/t_c \rightarrow 0$ the coupling of the adatom 1 to the STM is negligible compared to the tip-host coupling. The achievement of this regime can be reliable by the employment of an atom with deeply localized orbital. Such an orbital is characterized by a wave function which is more compact than that of carbon atoms, thus preventing that the hopping term t_{d1} becomes dominant.

After some algebra [26], Eq.(7) can be reduced to

$$\begin{aligned} \Psi_{\sigma}(\mathbf{R} = \mathbf{0}) &= \frac{1}{2\pi} \sqrt{\frac{\pi\Omega_0}{\mathcal{N}}} \sum_{ns} \int \left(\frac{\hbar v_F k}{-t} \right) \sqrt{|k|} dk c_{n,sk\sigma} \\ &\equiv \Psi_{\text{phantom},\sigma}, \end{aligned} \quad (9)$$

which corresponds to the fermionic operator describing the quantum state of the fictitious or phantom atom placed in the center of the hexagonal cell, where n runs over the Dirac points $\mathbf{K}_{\pm} = 2\pi/3a(1, \pm 1/\sqrt{3})$.

By applying the linear response theory, in which the STM tip is considered as a probe, it is possible to show that the differential conductance is determined by

$$G(\mathbf{R}) \sim \frac{e^2}{h} \pi \Gamma_{\text{tip}} \text{LDOS}(\mathbf{R}), \quad (10)$$

where e is the electron charge, $\Gamma_{\text{tip}} = 4\pi t_c^2 \rho_{\text{tip}}$, ρ_{tip} is the DOS for the tip and $\text{LDOS}(\mathbf{R})$ is the LDOS of the phantom atom perturbed by the adatoms, which despite being a local property it accounts for the entire bath composed by the phantom atoms. It is worth mentioning that if one increases the ratio t_{d1}/t_c in Eq.(8), one should treat the coupling to STM at the same footing as the coupling in “graphene+adatoms” system and as a result, the conductance is not simply proportional to the LDOS as predicted by the linear response theory (Eq.(10)). For the regime of strong coupling between adatom and STM tip, the theoretical framework found in Ref. [9] can be applied for the calculation of the conductance. However, as we do not expect the appearance of the BICs in this situation, its detailed analysis is outside the scope of the current work.

To obtain such a LDOS we first change the system Hamiltonian of Eq.(2) to the momenta domain by performing the transformation

$$\Psi_{s\sigma}(\mathbf{R}_m) = \frac{1}{\sqrt{\mathcal{N}}} \sum_{\mathbf{k}} e^{i\mathbf{k}\cdot\mathbf{R}_m} c_{s\mathbf{k}\sigma}, \quad (11)$$

with \mathcal{N} as the total number of states, $c_{A\mathbf{k}\sigma} = a_{\mathbf{k}\sigma}$ and $c_{B\mathbf{k}\sigma} = b_{\mathbf{k}\sigma}$, which yields the Hamiltonian:

$$\begin{aligned} \mathcal{H}_{2D} = & -t \sum_{\mathbf{k}\sigma} [\phi(\mathbf{k}) a_{\mathbf{k}\sigma}^\dagger b_{\mathbf{k}\sigma} + \text{H.c.}] + \sum_{j\sigma} \mathcal{E}_{jd\sigma} n_{d_j\sigma} \\ & + \mathcal{U} \sum_j n_{d_j\uparrow} n_{d_j\downarrow} + \mathcal{V} \sum_{j\sigma} [\Psi_\sigma(\mathbf{R}=\mathbf{0}) d_{j\sigma}^\dagger + \text{H.c.}], \end{aligned} \quad (12)$$

where

$$\Psi_\sigma(\mathbf{R}) = \frac{1}{\sqrt{\mathcal{N}}} \sum_{\mathbf{k}} e^{i\mathbf{k}\cdot\mathbf{R}} (\phi(\mathbf{k}) a_{\mathbf{k}\sigma} + \phi^*(\mathbf{k}) b_{\mathbf{k}\sigma}) \quad (13)$$

and $\phi(\mathbf{k}) = \sum_{i=1}^3 e^{i\mathbf{k}\cdot\delta_i}$.

Next we introduce the retarded Green's function in time domain τ

$$\mathcal{G}_\sigma(\mathbf{R}, \tau) = -\frac{i}{\hbar} \theta(\tau) \text{Tr}\{\rho_{2D} [\tilde{\Psi}_\sigma(\mathbf{R}, \tau), \tilde{\Psi}_\sigma^\dagger(\mathbf{R}, 0)]_+\}, \quad (14)$$

where $\theta(\tau)$ is the Heaviside function, ρ_{2D} is the density matrix of the system described by the Hamiltonian of Eq.(2) and $[\dots]_+$ is the anticommutator between operators taken in the Heisenberg picture.

Therefore, the LDOS can be obtained as

$$\text{LDOS}(\mathbf{R}) = -\frac{1}{\pi} \text{Im} \left[\sum_{\sigma} \tilde{\mathcal{G}}_\sigma(\mathbf{R}, \mathcal{E}^+) \right], \quad (15)$$

where $\tilde{\mathcal{G}}_\sigma(\mathbf{R}, \mathcal{E}^+)$ is the time Fourier transform of $\mathcal{G}_\sigma(\mathbf{R}, \tau)$. Then by applying the equation of motion (EOM) to the $\mathcal{G}_\sigma(\mathbf{R}, \tau)$, one can show that near the Dirac points where $t|\phi(\mathbf{k})| = \hbar v_F k$ one has:

$$\begin{aligned} \text{LDOS}(\mathbf{R}) &= 2\mathcal{D}_0 + \Delta \text{LDOS}(\mathbf{R}) = \\ &= 2\mathcal{D}_0 + \sum_{jl} \Delta \text{LDOS}_{jl}(\mathbf{R}). \end{aligned} \quad (16)$$

Here

$$\mathcal{D}_0 \equiv \mathcal{D}_0^{\text{phantom}} = \frac{1}{\mathcal{N}} \frac{\Omega_0}{\pi (\hbar v_F)^2} \frac{|\mathcal{E}|^3}{t^2} \quad (17)$$

corresponds to the DOS of the fictitious lattice of so-called phantom atoms as depicted in Fig.1(a). It is worth noticing that such a DOS is spatially independent as expected for a translational invariant system, thus revealing that the aforementioned lattice is periodic over a set of phantom atoms and encloses all energy continuum. This DOS is expressed in terms of the Fermi velocity v_F and the unit cell area Ω_0 .

The induced density of states reads

$$\begin{aligned} \Delta \text{LDOS}_{jl}(\mathbf{R}) &= -\Delta \mathcal{D}_0 \sum_{\sigma} \text{Im}\{[q_j(\mathbf{R}) - i\mathcal{F}_j(\mathbf{R})] \tilde{\mathcal{G}}_{d_{l\sigma}d_{j\sigma}} \\ &\quad \times [q_l(-\mathbf{R}) - i\mathcal{F}_l(-\mathbf{R})]\}. \end{aligned} \quad (18)$$

It is coordinate dependent, which is a clear consequence of the breaking of the periodicity of the phantom lattice due to the presence of the adatoms. Clearly, it depends on the Green's functions of the adatoms, namely $\mathcal{G}_{d_{l\sigma}d_{j\sigma}}$ ($j, l = 1, 2$), which can be obtained by determining the time Fourier transform of

$$\mathcal{G}_{d_{l\sigma}d_{j\sigma}}(\tau) = -\frac{i}{\hbar} \theta(\tau) \text{Tr}\{\rho_{2D} [d_{l\sigma}(\tau), d_{j\sigma}^\dagger(0)]_+\}. \quad (19)$$

Eq.(18) also depends on the position \mathbf{R} of the phantom atom, the Anderson broadening $\Delta = \pi \mathcal{D}_0^{\text{phantom}} \mathcal{V}^2 \propto |\mathcal{E}|^3$, which according to Ref.[9] arises from adatoms with electronic orbitals obeying the C_{3v} group symmetry as for instance the cases s , f_{z^3} and d_{z^2} .

$$q_j(\mathbf{R}) = \frac{1}{\Delta} \text{Re} \Sigma_{\text{phantom}}(\mathbf{R}) + \delta_{j1} (\pi \Delta \mathcal{D}_0)^{-1/2} (t_{d1}/t_c) \quad (20)$$

is the Fano factor that characterizes the interference between the direct adatom-host and STM-host paths [13] defined by the ratio t_{d1}/t_c . The factor $\mathcal{F}_j(\mathbf{R})$ reads:

$$\mathcal{F}_j(\mathbf{R}) = -\frac{1}{\Delta} \text{Im} \Sigma_{\text{phantom}}(\mathbf{R}), \quad (21)$$

where

$$\Sigma_{\text{phantom}}(\mathbf{R}) = \frac{2\mathcal{V}^2}{\mathcal{N}} \sum_{\mathbf{k}} \frac{e^{-i\mathbf{k}\cdot\mathbf{R}} \mathcal{E} + |\phi(\mathbf{k})|^2}{\mathcal{E} + 2 - t^2 |\phi(\mathbf{k})|^2} \quad (22)$$

is the self-energy, which at $\mathbf{R} = \mathbf{0}$ and near the Dirac points can be approximated by

$$\Sigma_{\text{phantom}}(\mathbf{R} = \mathbf{0}) = 2\nu^2 \frac{\mathcal{E}}{D^2 t^2} (\mathcal{E}^2 \ln \left| \frac{\mathcal{E}^2}{D^2 - \mathcal{E}^2} \right| - D^2) - i\Delta \quad (23)$$

as it was originally derived in Refs. [8] and [9] ($D \approx 7\text{eV}$ denotes the band-edge).

From the point of view of the STM-host coupling, a phantom atom emulates a single site beneath the STM tip. Note that the \mathcal{D}_0 of Eq.(17) differs from the standard DOS of graphene in the situation of a single carbon connected to a tip, which is characterized by $\mathcal{D}_0^{\text{carbon}} = \Omega_0 |\mathcal{E}| / 2\mathcal{N}\pi (\hbar v_F)^2$. The cubic dependence $\sim |\mathcal{E}|^3$ at low energies for the phantom DOS arises from the quantum interference between the electron paths through the hexagonal cell: the straight aftermath of such a process is the modification of the band-structure of graphene, thus distorting the well-known linear behavior for the DOS when the STM tip position coincides with the center of the hexagon.

To determine the density of states DOS_{jj} of the adatoms at the site $\mathbf{R} = \mathbf{0}$ of the host we should calculate the Green's functions $\tilde{\mathcal{G}}_{d_{j\sigma}d_{j\sigma}}$:

$$DOS_{jj} = -\frac{1}{\pi} \text{Im} \left(\sum_{\sigma} \tilde{\mathcal{G}}_{d_{j\sigma}d_{j\sigma}} \right). \quad (24)$$

To this end, the Hubbard I approximation can be used [25]. This approach provides reliable results away from the Kondo regime [27]. We start by employing the equation-of-motion (EOM) method to a single particle retarded Green's function of Eq.(19) in time domain for an adatom. Going to energy domain one gets:

$$(\mathcal{E}^+ - \mathcal{E}_{ld\sigma}) \tilde{\mathcal{G}}_{d_{l\sigma}d_{j\sigma}} = \delta_{lj} + \Sigma_{\text{phantom}}(\mathbf{R} = \mathbf{0}) \sum_{\bar{l}} \tilde{\mathcal{G}}_{d_{\bar{l}\sigma}d_{j\sigma}} + \mathcal{U} \tilde{\mathcal{G}}_{d_{l\sigma}n_{d_{l\bar{\sigma}}},d_{j\sigma}}, \quad (25)$$

with $\mathcal{E}^+ = \mathcal{E} + i0^+$. In the equation above, $\tilde{\mathcal{G}}_{d_{l\sigma}n_{d_{l\bar{\sigma}}},d_{j\sigma}}$ denotes a two particle Green's function composed by four fermionic operators, obtained by the Fourier transform of

$$\mathcal{G}_{d_{l\sigma}n_{d_{l\bar{\sigma}}},d_{j\sigma}} = -\frac{i}{\hbar} \theta(\tau) \text{Tr} \{ \rho_{2D} [d_{l\sigma}(\tau) n_{d_{l\bar{\sigma}}}(\tau), d_{j\sigma}^\dagger(0)]_+ \}, \quad (26)$$

where $\bar{\sigma} = -\sigma$ and $n_{d_{l\bar{\sigma}}} = d_{l\bar{\sigma}}^\dagger d_{l\bar{\sigma}}$. In order to close the system of the dynamic equations, we obtain the EOM for the Green's function $\tilde{\mathcal{G}}_{d_{l\sigma}n_{d_{l\bar{\sigma}}},d_{j\sigma}}$, which reads:

$$(\mathcal{E}^+ - \mathcal{E}_{ld\sigma} - \mathcal{U}) \tilde{\mathcal{G}}_{d_{l\sigma}n_{d_{l\bar{\sigma}}},d_{j\sigma}} = \delta_{lj} \langle n_{d_{l\bar{\sigma}}} \rangle + \sum_{\mathbf{k}s} \frac{\nu}{\sqrt{\mathcal{N}}} [-\phi_s(\mathbf{k}) \tilde{\mathcal{G}}_{c_{s\mathbf{k}\sigma}^\dagger d_{l\bar{\sigma}} d_{l\sigma}, d_{j\sigma}} + \phi_s^*(\mathbf{k}) (\tilde{\mathcal{G}}_{c_{s\mathbf{k}\sigma} d_{l\bar{\sigma}}^\dagger d_{l\sigma}, d_{j\sigma}} + \tilde{\mathcal{G}}_{d_{l\bar{\sigma}}^\dagger c_{s\mathbf{k}\sigma} d_{l\sigma}, d_{j\sigma}})], \quad (27)$$

where the index $s = A, B$ marks a sublattice, $c_{A\mathbf{k}\sigma} = a_{\mathbf{k}\sigma}$ and $c_{B\mathbf{k}\sigma} = b_{\mathbf{k}\sigma}$, $\phi_A(\mathbf{k}) = \phi^*(\mathbf{k})$ and $\phi_B(\mathbf{k}) = \phi(\mathbf{k})$,

expressed in terms of new Green's functions of the same order of $\tilde{\mathcal{G}}_{d_{l\sigma}n_{d_{l\bar{\sigma}}},d_{j\sigma}}$ and the occupation number can be determined as

$$\langle n_{d_{l\bar{\sigma}}} \rangle = -\frac{1}{\pi} \int_{-D}^{+D} n_F(\mathcal{E}) \text{Im}(\tilde{\mathcal{G}}_{d_{l\bar{\sigma}}d_{l\bar{\sigma}}}) d\mathcal{E}, \quad (28)$$

with $n_F(\mathcal{E})$ as the Fermi-Dirac distribution.

Our approach holds for temperatures $T \gg T_K$ (above the Kondo temperature). However, the temperature should not be very high in order that we can safely employ the Heaviside step function for the Fermi-Dirac distribution $n_F(\mathcal{E})$ [7]. By employing the Hubbard I approximation, we decouple the Green's functions in the right-hand side of Eq.(27), as follows: $\tilde{\mathcal{G}}_{c_{s\mathbf{k}\sigma}^\dagger d_{l\bar{\sigma}} d_{l\sigma}, d_{j\sigma}} \simeq \langle c_{s\mathbf{k}\sigma}^\dagger d_{l\bar{\sigma}} \rangle \tilde{\mathcal{G}}_{d_{l\sigma}d_{j\sigma}}$ and $\tilde{\mathcal{G}}_{d_{l\bar{\sigma}}^\dagger c_{s\mathbf{k}\sigma} d_{l\sigma}, d_{j\sigma}} \simeq \langle c_{s\mathbf{k}\sigma}^\dagger d_{l\bar{\sigma}} \rangle \tilde{\mathcal{G}}_{d_{l\sigma}d_{j\sigma}}$, where we have used $\sum_{\mathbf{k}s} \phi(\mathbf{k}) = \sum_{\mathbf{k}s} \phi^*(\mathbf{k})$. As a result, we find

$$(\mathcal{E}^+ - \mathcal{E}_{ld\sigma} - \mathcal{U}) \tilde{\mathcal{G}}_{d_{l\sigma}n_{d_{l\bar{\sigma}}},d_{j\sigma}} = \delta_{lj} \langle n_{d_{l\bar{\sigma}}} \rangle + \frac{\nu_j}{\sqrt{\mathcal{N}}} \sum_{\mathbf{k}s} \phi_s^*(\mathbf{k}) \tilde{\mathcal{G}}_{c_{s\mathbf{k}\sigma} d_{l\bar{\sigma}}^\dagger d_{l\sigma}, d_{j\sigma}}. \quad (29)$$

To complete the calculation, we need to determine $\tilde{\mathcal{G}}_{c_{s\mathbf{k}\sigma} d_{l\bar{\sigma}}^\dagger d_{l\sigma}, d_{j\sigma}}$. Once again, employing the EOM approach for $\tilde{\mathcal{G}}_{c_{s\mathbf{k}\sigma} d_{l\bar{\sigma}}^\dagger d_{l\sigma}, d_{j\sigma}}$, we obtain

$$\begin{aligned} \mathcal{E}^+ \tilde{\mathcal{G}}_{c_{s\mathbf{k}\sigma} d_{l\bar{\sigma}}^\dagger d_{l\sigma}, d_{j\sigma}} &= -t\phi_{\bar{s}}(\mathbf{k}) \tilde{\mathcal{G}}_{c_{\bar{s}\mathbf{k}\sigma} d_{l\bar{\sigma}}^\dagger d_{l\sigma}, d_{j\sigma}} \\ &+ \sum_{\mathbf{q}\bar{s}} \frac{\nu_l}{\sqrt{\mathcal{N}}} \phi_{\bar{s}}^*(\mathbf{q}) \tilde{\mathcal{G}}_{c_{s\mathbf{k}\sigma} d_{l\bar{\sigma}}^\dagger c_{\bar{s}\mathbf{q}\bar{\sigma}}, d_{j\sigma}} \\ &+ \sum_j \frac{\nu_j}{\sqrt{\mathcal{N}}} \phi_s(\mathbf{k}) \tilde{\mathcal{G}}_{d_{j\sigma}n_{d_{l\bar{\sigma}}}, d_{j\sigma}} \\ &- \sum_{\mathbf{q}\bar{s}} \frac{\nu_l}{\sqrt{\mathcal{N}}} \phi_{\bar{s}}(\mathbf{q}) \tilde{\mathcal{G}}_{c_{s\mathbf{k}\sigma}^\dagger d_{l\bar{\sigma}} c_{\bar{s}\mathbf{q}\bar{\sigma}}, d_{j\sigma}}, \end{aligned} \quad (30)$$

where $\bar{s} = A, B$ respectively for $s = B, A$ as labels to correlate simultaneously distinct sublattices, while $\bar{s} = A, B$ runs arbitrarily.

In a similar way by using Hubbard I scheme for Eq.(30) we have $\tilde{\mathcal{G}}_{c_{s\mathbf{k}\sigma} d_{l\bar{\sigma}}^\dagger c_{\bar{s}\mathbf{q}\bar{\sigma}}, d_{j\sigma}} \simeq \langle d_{l\bar{\sigma}}^\dagger c_{\bar{s}\mathbf{q}\bar{\sigma}} \rangle \tilde{\mathcal{G}}_{c_{s\mathbf{k}\sigma} d_{j\sigma}}$, $\tilde{\mathcal{G}}_{c_{s\mathbf{k}\sigma}^\dagger d_{l\bar{\sigma}} c_{\bar{s}\mathbf{q}\bar{\sigma}}, d_{j\sigma}} \simeq \langle d_{l\bar{\sigma}}^\dagger c_{\bar{s}\mathbf{q}\bar{\sigma}} \rangle \tilde{\mathcal{G}}_{c_{s\mathbf{k}\sigma} d_{j\sigma}}$ and $\tilde{\mathcal{G}}_{d_{j\sigma}n_{d_{l\bar{\sigma}}}, d_{j\sigma}} \simeq \langle n_{d_{l\bar{\sigma}}} \rangle \tilde{\mathcal{G}}_{d_{j\sigma}d_{j\sigma}}$, which in combination with Eqs. (25) and (29) results in

$$\tilde{\mathcal{G}}_{d_{j\sigma}d_{j\sigma}} = \frac{\lambda_j^{\bar{\sigma}}}{\mathcal{E} - \mathcal{E}_{jd\sigma} - \tilde{\Sigma}_{jj}^{\bar{\sigma}}}, \quad (31)$$

where $\lambda_j^{\bar{\sigma}} = (1 + \frac{\mathcal{U} \langle n_{d_{j\bar{\sigma}}} \rangle}{\mathcal{E} - \mathcal{E}_{jd\sigma} - \mathcal{U} - \Sigma_{\text{phantom}}(\mathbf{R} = \mathbf{0})})$, and

$$\tilde{\Sigma}_{jj}^{\sigma} = \Sigma(\mathbf{R} = \mathbf{0}) + \lambda_{\bar{j}}^{\sigma} \lambda_{\bar{j}}^{\sigma} \frac{[\Sigma_{\text{phantom}}(\mathbf{R} = \mathbf{0})]^2}{\mathcal{E} - \mathcal{E}_{\bar{j}d\sigma} - \Sigma_{\text{phantom}}(\mathbf{R} = \mathbf{0})} \quad (32)$$

is the total self-energy, with $\bar{j} = 2, 1$ respectively for $j = 1, 2$ for the indexes corresponding to distinct adatoms and

$$\tilde{\mathcal{G}}_{d_{j\sigma}d_{\bar{j}\sigma}} = \frac{\lambda_{\bar{j}}^{\sigma} \Sigma_{\text{phantom}}(\mathbf{R} = \mathbf{0}) \tilde{\mathcal{G}}_{d_{\bar{j}\sigma}d_{\bar{j}\sigma}}}{\mathcal{E} - \mathcal{E}_{j d\sigma} - \Sigma_{\text{phantom}}(\mathbf{R} = \mathbf{0})} \quad (33)$$

are mixed Green's functions, which describe the correlations between the adatoms and are responsible for Fano destructive interference.

III. RESULTS AND DISCUSSION

In the discussion below we adopt the following set of the system parameters: $t_{d1}/t_c = 10^{-6}$, which ensures the assumption of the STM tip acting as a probe of the “graphene+adatoms” system LDOS as discussed in Sec.II, $\mathcal{E}_d = -0.07D$, $\mathcal{U} = 0.14D$, $\mathcal{V} = 0.14D$ and $v_F \approx c/300$ [7].

Panel (a) of the Fig.2 shows the comparison between the linear LDOS of graphene (green curve) versus D_0^{phantom} with cubic dependence characteristic for the phantom atom of Eq.(17) (blue curve). Fig.2(b) displays the densities of states of the adatoms $\text{DOS}_{jj} = \text{DOS}_{11} = \text{DOS}_{22}$ defined by Eq.(24) with zero detuning ($\Delta\mathcal{E} = 0$), where two peaks labeled as (1) and (2) are situated within the valence band ($\mathcal{E} < \mathcal{E}_F \equiv 0$) for the case of $\mathcal{U} \neq 0$ (red curve). Two extra peaks appear within the conduction band ($\mathcal{E} > \mathcal{E}_F \equiv 0$) as well (not shown), since we assumed the symmetric Anderson model with the constraint $2\mathcal{E}_d + \mathcal{U} = 0$ being fulfilled. In this regime, the graphene Hamiltonian with adatoms is invariant under particle-hole transformation, and all the properties of the peaks within the conduction band are the same as those within the valence band, thus we do not need to perform separate analysis for them. Note, that deviations from the condition $2\mathcal{E}_d + \mathcal{U} = 0$ will not change the presented results qualitatively, but positions of the peaks in conduction and valence bands will not be anymore symmetric. For comparison we also present the curve for $\mathcal{U} = 0$ (dark-dotted curve), characterized by a single peak labeled as (3).

Panel (c) of the Fig.2 shows the contributions of the adatoms to the LDOS of graphene. For $\mathcal{U} \neq 0$ the diagonal term $\Delta\text{LDOS}_{jj} = \Delta\text{LDOS}_{11} = \Delta\text{LDOS}_{22}$ displays pronounced peaks at the same energies as the DOS of the adatoms shown at the panel (b). On the contrary, the mixing term $\Delta\text{LDOS}_{jl} = \Delta\text{LDOS}_{12} = \Delta\text{LDOS}_{21}$ exhibits sharp Fano dip corresponding to the peak located around $\mathcal{E} \approx -6.3 \times 10^{-2}D$. When all contributions to the LDOS are added, this antiresonance cancels exactly the corresponding resonance in the diagonal term. This means that the peak (1) of panel (b) can be considered

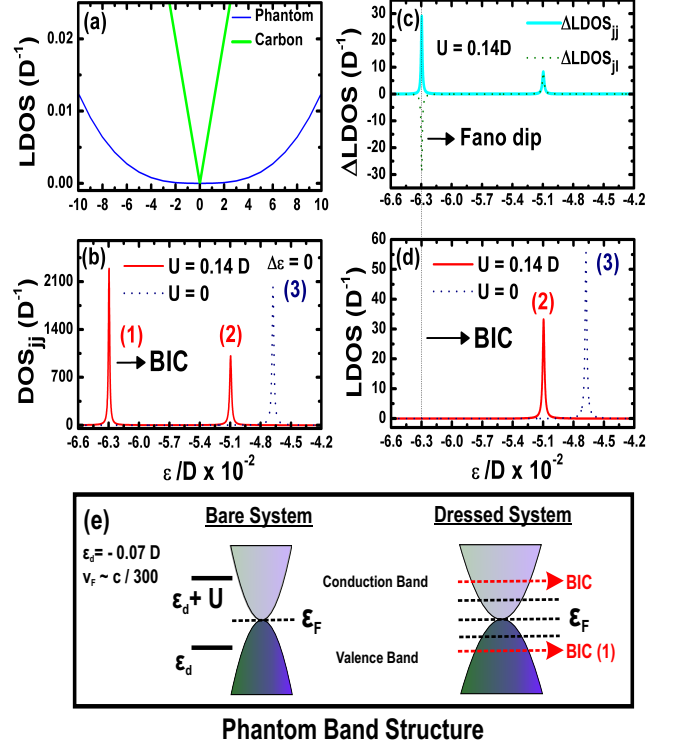


Figure 2. (Color online) (a) LDOS of graphene coupled to STM tip for two configurations: the tip above the carbon atom of graphene (labeled as carbon) and the tip in the center of the hexagonal lattice (labeled as phantom). (b) Density of states for the pair of adatoms $\text{DOS}_{jj} = \text{DOS}_{11} = \text{DOS}_{22}$ within the valence band. The parameters are $\mathcal{E}_d = -0.07D$, $\mathcal{U} = 0.14D$, $\mathcal{V} = 0.14D$, $v_F \approx c/300$ and $\Delta\mathcal{E} = 0$. Additional two peaks in the conduction band are symmetrically placed if the condition $2\mathcal{E}_d + \mathcal{U} = 0$ is satisfied, which are not shown. (c) Contributions to the LDOS of graphene from the adatom pair. Diagonal contribution shows two pronounced peaks, while mixing term shows a single pronounced antiresonance. (d) Total LDOS revealing the BIC (marked by vertical line) at position where the resonance of the diagonal term in the LDOS is compensated by the antiresonance in the mixing term. (e) Sketch of the energy diagram of the system. Left: energy levels without the dressing of the adatoms by conducting electrons. Right: the energy diagram accounting for the Coulomb dressing. The pair of BICs is indicated by red arrows. In both of right and left panels the coupling of the graphene sheet to the STM tip turns the linear $|\mathcal{E}|$ dependence within the density of states of the host into cubic one ($|\mathcal{E}|^3$).

as a BIC arising from a Fano destructive interference assisted by Coulomb correlations: in the situation of finite Coulomb potential \mathcal{U} , ΔLDOS_{jl} for $j \neq l$ describes electronic waves that travel forth and back between the upper and lower adatoms, which for a given energy \mathcal{E} , become phase shifted by π with respect to the waves scattered by the adatoms enclosed by ΔLDOS_{jj} . Particularly at the sites of the adatoms where the BICs lie

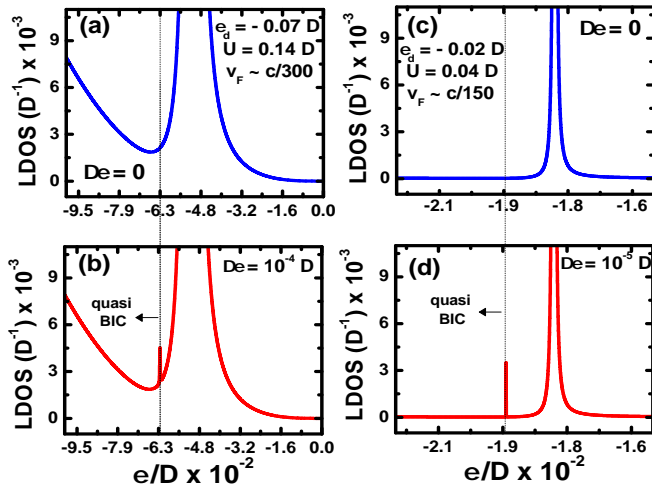


Figure 3. (Color online) (a) $\mathcal{E}_d = -0.07D$, $\mathcal{U} = 0.14D$, $\mathcal{V} = 0.14D$, $v_F \approx c/300$ and $\Delta\mathcal{E} = 0$: LDOS in the region around the position of the BIC. The latter lies at $\mathcal{E} \approx -6.3 \times 10^{-2}D$ and is invisible in the LDOS, its position is shown by a vertical line. (b) The LDOS in the region around the position of the BIC for non-zero detuning between the energies of the upper and lower adatoms $\Delta\mathcal{E} = 10^{-4}D$, all other parameters are the same as in panel (a). One clearly sees that the BIC is reflected in the LDOS in form of a tiny peak at $\mathcal{E} \approx -6.3 \times 10^{-2}D$ and thus should become detectable in transport measurements. (c) Same as panel (a), but for the different values of parameters: $\mathcal{E}_d = -0.02D$, $\mathcal{U} = 0.04D$ and $v_F \approx c/150$. (d) The LDOS in the region around the position of the BIC for non-zero detuning between the energies of the upper and lower adatoms $\Delta\mathcal{E} = 10^{-5}D$, all other parameters are the same as in panel (c).

and with $\mathcal{E} \approx -6.3 \times 10^{-2}D$, such a condition is fulfilled and is reflected by the peak and Fano dip, respectively in $\Delta\text{LDOS}_{11} = \Delta\text{LDOS}_{22}$ and $\Delta\text{LDOS}_{12} = \Delta\text{LDOS}_{21}$ as found in Fig.2(c).

We highlight that the peak in the DOS marked as peak (1) in Fig. 2(b) appearing around $\mathcal{E} \approx -6.3 \times 10^{-2}D$ in the red curve does not rise at the same position in the LDOS of panel (d) due to the Fano suppression mechanism, thus preventing the revealing of the BIC by a conductance measurement. This feature is made explicit by the vertical line crossing both panels (c) and (d) of Fig.2, where the BIC position is marked. We checked that for $\mathcal{U} = 0$ BICs do not appear. For reference purposes we showed the corresponding peak labeled as (3) in Figs.2(b) and (d). In Fig.2(e), the band structure of the phantom atoms in the presence of BICs is depicted.

In Fig.3(a) we have the enlargement of the region wherein the peak around $\mathcal{E} \approx -6.3 \times 10^{-2}D$ is absent in the LDOS of Fig.2(d), thus suggesting the existence of a BIC at this position. To make this BIC observable, one needs to introduce the coupling between it and the continuum states, which can be achieved by the introduction of a small detuning $\Delta\mathcal{E}$ between the energies of the upper

and lower adatoms. As a matter of fact, this detuning will appear automatically due to the hybridizations of the STM tip with the adatoms, in particular when the former is found closer to the latter. In Fig.3(b) we plot the LDOS for $\Delta\mathcal{E} = 10^{-4}D$. One clearly sees that visible, although rather weak peak appears at the energy corresponding to the BIC, in which a true BIC is transformed to a quasi-BIC detectable in transport experiments. Here we stress that within our theoretical framework, the role of the detuning $\Delta\mathcal{E}$ is the emulation of nonperturbative values for the ratio t_{d1}/t_c , which forces the leaking of the BIC into the system energy continuum as the aftermath of the renormalization made by the STM tip on the level of the upper adatom. We should emphasize that Eq.(16) that describes this energy continuum as well as the conductance G through the system via Eq.(10), enclose fingerprints arising from Eq.(24) for the adatoms, as for instance, the quasi-BIC nearby $\mathcal{E} \approx -6.3 \times 10^{-2}D$ observed in Fig.3(b). This narrow state corresponds to that denoted by the resonance labeled as (1) in Fig.2(b) that leaks into the continuum of the system.

In the opposite situation where $\Delta\mathcal{E} = 0$, such a decay of the BIC is prevented due to the mechanism of Fano destructive interference pointed out previously. Thus Eq.(16) contains just the background contribution of Eq.(17) at $\mathcal{E} \approx -6.3 \times 10^{-2}D$ as Fig.3(a) shows. In this case, the LDOS of the “graphene+adatoms” system behaves as that for the lattice of phantom atoms without adatoms. Thereby, if sharp resonances appear in both Eqs.(16) and (24) at the same position, they reveal the decay of the state within the adatoms into the energy continuum of the system: the sharp resonance appearing in the former equation is then considered a quasi-BIC. A quasi-BIC is characterized by a sharp resonance in Eq.(16) being detectable by the conductance G of Eq.(10), which indeed describes at $\mathcal{E} \approx -6.3 \times 10^{-2}D$ an electron that spends a long time in the vicinity of the adatom, whose wave function behaves as a Bloch state away from such a site.

Additionally, we clarify that a BIC is represented by the resonance belonging to the adatom under consideration since it appears via its DOS given by Eq.(24), but is absent in Eq.(16) that determines the system conductance. It is worth noticing that despite the small but finite width $\Delta \propto |\mathcal{E}|^3$ of such a state in Eq.(24), which is visible around $\mathcal{E} \approx -6.3 \times 10^{-2}D$ in Fig.2(b), the Fano destructive interference mechanism revealed in this work ensures that the state level is embedded in the continuum. This situation corresponds to electrons fully trapped within these adatoms in such a way that the decay rate $\sim \Delta/\hbar$ is suppressed.

On the other hand, the visibility of the quasi-BIC peak can be improved by approaching both levels \mathcal{E}_d and \mathcal{U} towards the Dirac points ($\mathcal{E}_d = -0.02D$ and $\mathcal{U} = 0.04D$) combined with the increasing of the Fermi velocity v_F ($v_F \approx c/150$) as shown at panels (c) and (d) of the same figure. From the experimental perspective the tuning of the Fermi velocity can be performed by changing the di-

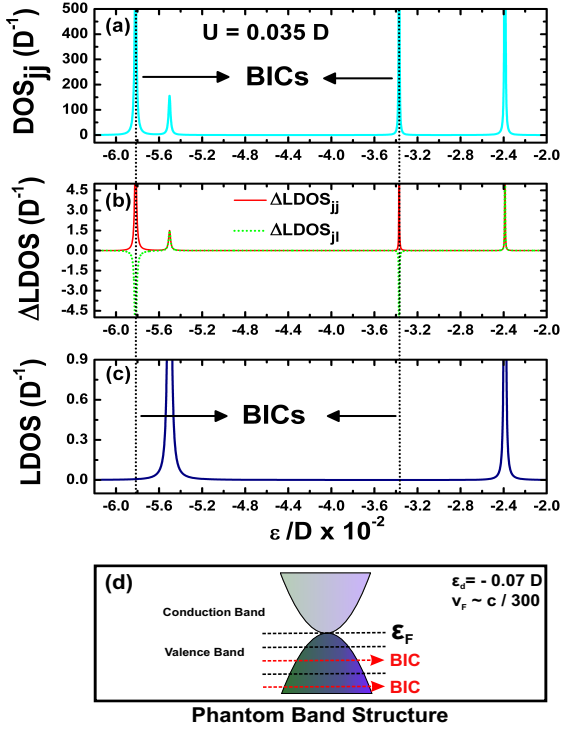


Figure 4. (Color online) (a) Density of states for the pair of adatoms $DOS_{jj} = DOS_{11} = DOS_{22}$ within the valence band. The parameters are $\mathcal{E}_d = -0.07D$, $\mathcal{U} = 0.035D$, $\mathcal{V} = 0.14D$, $v_F \approx c/300$ and $\Delta\mathcal{E} = 0$. Four peaks are present within the valence band, as $2\mathcal{E}_d + \mathcal{U} \neq 0$ particle-hole symmetry is broken. (b) Contributions to the LDOS of graphene from the adatom pair. Diagonal contribution shows four pronounced peaks, while mixing term shows a couple of pronounced antiresonances. (c) Total LDOS revealing the BICs (marked by vertical lines) at positions where resonances of the diagonal term in the LDOS are compensated by the antiresonances in the mixing term. (d) Sketch of the energy diagram of the system.

electric constant in the substrate hosting the graphene sheet [28, 29]. We should point out that the assumption of considering adatoms slightly off resonance, due to a detuning in energy levels for detection of quasi-BICs, was adopted in Ref. [23] for graphene ribbons. Here we apply the same procedure on our “graphene+adatoms” system in order to induce the decay of the BICs within the adatoms into the continuum of the aforementioned system.

In Fig.4 we present the results for the case of the broken particle-hole symmetry, taking $\mathcal{U} = 0.035D$, $\mathcal{E}_d = -0.07D$, $v_F \approx c/300$ and $\Delta\mathcal{E} = 0$. By decreasing the Coulomb correlation energy from $\mathcal{U} = 0.14D$ to $\mathcal{U} = 0.035D$, it is possible to shift the peaks found within the conduction band ($\mathcal{E} > \mathcal{E}_F \equiv 0$) for the symmetric case $2\mathcal{E}_d + \mathcal{U} = 0$ into the valence band ($\mathcal{E} < \mathcal{E}_F \equiv 0$) as demonstrated at the panel (a). Thus instead of the couple

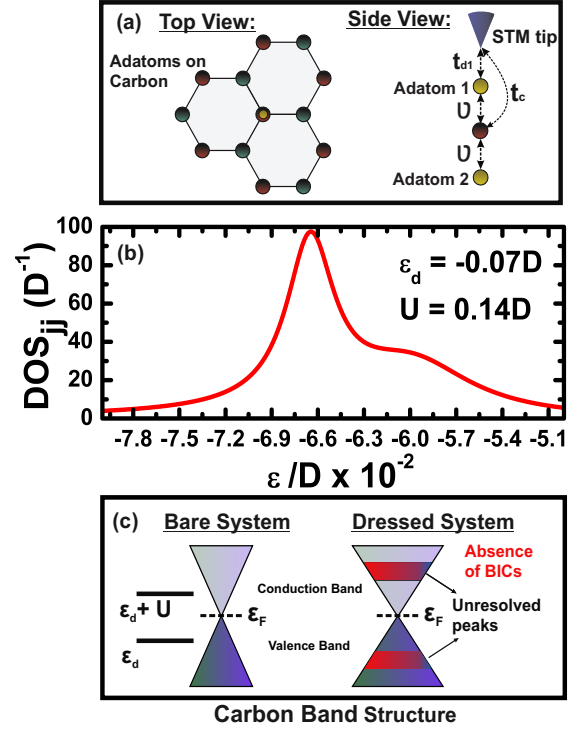


Figure 5. (Color online) (a) Adatoms aligned with one of the carbon atoms. (b) $\mathcal{E}_d = -0.07D$, $\mathcal{U} = 0.14D$, $\mathcal{V} = 0.14D$, $v_F \approx c/300$ and $\Delta\mathcal{E} = 0$: $DOS_{jj} = DOS_{11} = DOS_{22}$ of the adatoms in which unresolved peaks emerge, thus attesting that BICs can not be formed in such a geometry. (c) Dirac cones persist exhibiting unresolved resonances simultaneously within the valence and conduction bands.

of peaks found in Fig.2(b), four resonances appear within the valence band. Although the condition $2\mathcal{E}_d + \mathcal{U} = 0$ is not any more satisfied, the underlying Physics remains: BICs emerge due to Fano antiresonances in the mixing term of the LDOS that suppress the corresponding peaks found in the diagonal term (see panels (a), (b) and (c) in which BICs are identified by vertical lines). Panel (d) shows the band structure in such a case.

Fig.5 depicts the analysis of the situation in which the adatoms are aligned with one of the carbon atoms of the lattice as shown in the panel (a). The parameters are the same employed in Fig.2. One can find the expression for the LDOS using the field operator of a carbon atom [26]

$$\Psi_{\text{carbon},\sigma} = \frac{1}{2\pi} \sqrt{\frac{\pi\Omega_0}{\mathcal{N}}} \sum_n \int \sqrt{|k|} dk c_{nk\sigma}, \quad (34)$$

instead of the field operator of a phantom atom given by Eq.(9). The resulting LDOS is given by the same expressions of the Eqs.(16) and (18), with only difference that now $\mathcal{D}_0 \equiv \mathcal{D}_0^{\text{carbon}} = \Omega_0 |\mathcal{E}| / 2N\pi (\hbar v_F)^2$, $\Delta = \pi \mathcal{D}_0^{\text{carbon}} \mathcal{V}^2$ and

$$\Sigma_{\text{carbon}}(\mathbf{R} = \mathbf{0}) = \frac{\mathcal{V}^2}{D^2} \mathcal{E} \ln \left| \frac{\mathcal{E}^2}{D^2 - \mathcal{E}^2} \right| - i\Delta \quad (35)$$

stands for the self-energy [7] instead of that found in Eq. (23) for the phantom atom.

Panel (b) shows the DOS for the considered situation. One clearly sees that differently from the case of the phantom atom BICs do not appear, since resolved peaks within $\text{DOS}_{jj} = \text{DOS}_{11} = \text{DOS}_{22}$ are absent and a couple of broad merged resonances appears instead. To explain such a behavior, let us focusing on the Anderson broadening Δ . For the case of a phantom atom $\Delta \propto |\mathcal{E}|^3$ and as the peaks at $\mathcal{E} \approx -6.3 \times 10^{-2}D$ and $\mathcal{E} \approx -5 \times 10^{-2}D$ denoted by (1) and (2) in Fig.2(b) are found nearby the Dirac points ($\mathcal{E} = 0$), they are narrow enough in this region and can be easily resolved. For the case of the collinear alinement of the impurities with one of the carbon atoms $\Delta \propto |\mathcal{E}|$, thereby the broadening of the peaks in the vicinity of the Dirac points increases and they become unresolved as seen at the Fig.5(b). Fig.5(c) displays the sketch of the Dirac cones in such a situation.

IV. CONCLUSIONS

In summary, we have demonstrated that BICs can appear in a system consisting of a graphene sheet and a

collinear pair of adatoms placed above and below the center of the hexagonal cell, where a fictitious or phantom atom emulates the six carbon atoms of the cell. The effect is due to the destructive Fano interference assisted by Coulomb correlations in the adatoms. We have checked that BICs do not appear if Coulomb interaction is absent or if adatoms are collinear with one of the carbon atoms in the lattice.

V. ACKNOWLEDGMENTS

This work was supported by the agencies CNPq, CAPES, 2014/14143-0 São Paulo Research Foundation (FAPESP), FP7 IRSES project QOCaN and Ran-nis project “Bose and Fermi systems for spintronics”. A. C. S. thanks the Nanyang Technological University at Singapore for hospitality.

-
- [1] K. S. Novoselov, *Rev. Mod. Phys.* **83**, 837 (2011).
 - [2] N. M. R. Peres, *Rev. Mod. Phys.* **82**, 2673 (2010).
 - [3] A.H. Castro Neto, F. Guinea, N. M. R. Peres, K. S. Novoselov, and A. K. Geim, *Rev. Mod. Phys.* **81**, 109 (2009).
 - [4] T. Eelbo, M. Wasniowska, M. Gyamfi, S. Forti, U. Starke, and R. Wiesendanger, *Phys.Rev.B* **87**, 205443 (2013).
 - [5] T. Eelbo, M. Wasniowska, P. Thakur, M. Gyamfi, B. Sachs, T. O. Wehling, S. Forti, U. Starke, C. Tieg, A. I. Lichtenstein, and R. Wiesendanger, *Phys. Rev. Lett.* **110**, 136804 (2013).
 - [6] X. Liu, C. Z. Wang, Y. X. Yao, W. C. Lu, M. Hupalo, M.C. Tringides, and K. M. Ho, *Phys. Rev. B* **83**, 235411 (2011).
 - [7] B. Uchoa, V. N. Kotov, N. M. R. Peres, and A. H. Castro Neto, *Phys. Rev. Lett.* **101**, 026805 (2008).
 - [8] B. Uchoa, L. Yang, S.-W.Tsai, N. M. R. Peres, and A. H. Castro Neto, *Phys. Rev. Lett.* **103**, 206804 (2009).
 - [9] B. Uchoa, L. Yang, S.-W.Tsai, N. M. R. Peres, and A. H. Castro Neto, *New J. Phys.* **16**, 013045 (2014).
 - [10] P. D. Gorman, J. M. Duffy, M. S. Ferreira, and S. R. Power, *Phys. Rev. B* **88**, 085405 (2013).
 - [11] E. Kogan, *Phys. Rev. B* **84**, 115119 (2013).
 - [12] M. Ternes, A. J. Heinrich, and W. -D. Schneider, *J. Phys.: Condens. Matter* **21**, 053001 (2009).
 - [13] A. E. Miroschnichenko, S. Flach, and Y. S. Kivshar, *Rev. Mod. Phys.* **82**, 2257 (2010).
 - [14] J. von Neumann and E. Wigner, *Phys. Z.* **30**, 465 (1929).
 - [15] F. H. Stillinger and D. R. Herrick, *Phys. Rev. A* **11**, 446 (1975).
 - [16] C. W. Hsu, B. Zhen, J. Lee, S.-L. Chua, S. G. Johnson, J. D. Joannopoulos, and M. Soljačić, *Nature* **499**, 188 (2013).
 - [17] Y. Boretz, G. Ordonez, S. Tanaka, and T. Petrosky, *Phys. Rev. A* **90**, 023853 (2014).
 - [18] Y. Plotnik, O. Peleg, F. Dreisow, M. Heinrich, S. Nolte, A. Szameit, and M. Segev, *Phys. Rev. Lett.* **107**, 183901 (2011).
 - [19] A. Crespi, L. Sansoni, G. D. Valle, A. Ciamei, R. Ramponi, F. Sciarrino, P. Mataloni, S. Longhi, and R. Osellame, *Phys. Rev. Lett.* **114**, 090201 (2015).
 - [20] J.M.-Petit and R.A. Molina, *Phys. Rev. B* **90**, 035434 (2014).
 - [21] G.D. Valle and S. Longhi, *Phys. Rev. B* **89**, 115118 (2014).
 - [22] C. González-Santander, P. A. Orellana, and F. Domínguez-Adame, *Europhys. Lett.* **102**, 17012 (2013).
 - [23] J. W. González, M. Pacheco, L. Rosales, and P. A. Orellana, *Europhys. Lett.* **91**, 66001 (2010).
 - [24] W.-J. Gong, X.-Y. Sui, Y. Wang, G.-D. Yu, and X.-H. Chen, *Nanoscale Research Letters* **8**, 330 (2013).
 - [25] J. Hubbard, *Proc. R. Soc. Lond. A*, **281**, 401 (1964).
 - [26] Z.-G. Zhu, K.-H. Ding, and J. Berakdar, *Europhys. Lett.* **90**, 67001 (2010).
 - [27] L. Li, Y.-Y. Ni, Y. Zhong, T.-F. Fang, and H.-G. Luo, *New J. Phys.* **15**, 053018 (2013).
 - [28] C. Hwang, D. A. Siegel, S.-K. Mo, W. Regan, A. Ismach, Y. Zhang, A. Zettl, and A. Lanzara, *Sci. Rep.* **2**, 590 (2012).
 - [29] D. A. Siegel, W. Regan, A. V. Fedorov, A. Zettl, and A. Lanzara, *Phys. Rev. Lett.* **110**, 146802 (2013).